Dynamic Event-Triggered Distributed Secondary Control of DC Microgrids

Yang-Yang Qian, *Member, IEEE*, Abhiram V. P. Premakumar, *Graduate Student Member, IEEE*, Yan Wan, *Senior Member, IEEE*, Zongli Lin, *Fellow, IEEE*, Yacov A. Shamash, *Life Fellow, IEEE*, and Ali Davoudi, *Senior Member, IEEE*

***Abstract*—Emerging distributed control paradigms rely on communication among converters of a microgrid. We investigate the secondary control of dc microgrids with a distributed dynamic event-triggering mechanism. The physical and cyber layers are represented by different graph topologies. To reduce the communication burden, a distributed dynamic event-triggering mechanism is designed. Therein, the Zeno behavior is excluded and in addition, a positive minimum interevent time (MIET) is determined. Asymptotic stability of the closed-loop system dynamics is proven, and the adjustment of the positive MIET is discussed. Compared to the existing static event-triggering mechanisms, the proposed dynamic one guarantees the existence of a positive MIET, whose value can be tuned by the design parameters. Controller/hardware-in-the-loop implementation results validate the efficacy of the proposed method.**

***Index Terms*—DC microgrids, distributed control, event-triggering mechanism (ETM), secondary control.**

I. Introduction

DIRECT current (dc) microgrids are gaining popularity due to the dc nature of emergent renewable energy sources, storage units, and electronics loads [1]–[3]. The basic control objectives of dc microgrids in the secondary control level include proportional load sharing and global voltage regulation [4], [5]. The proportional load sharing objective requires that all converters share the overall load current proportionally according to their current ratings. The global voltage regulation objective pertains to regulating the average voltage across the distributed line to a given set point. To simultaneously achieve these two objectives, distributed secondary control strategies in [4] and [5] require continuous information exchange among converters through a communication network.

Conventional periodic sampling control can cause unnecessary sampling and can increase the communication burden. A more efficient approach uses event-triggered control (ETC) [6], [7], where an event-triggering mechanism (ETM) decides when to execute controller updates and/or data sampling/transmission. Various ETMs have been developed for distributed secondary control of microgrids, e.g., [8]–[13]. An adaptive, centralized ETM [8] requires the global state of the closed-loop dynamics. Distributed ETMs are designed in [9]–[15], where the triggering threshold is state-dependent, and in [16], where the triggering threshold is time-dependent. These triggering mechanisms are static in the sense that the triggering condition depends on only system information (e.g., state or output) and/or time information without introducing any internal dynamic variable.

Dynamic ETMs have been introduced in [17] and [18] for single-agent systems and [19]–[21] for multiagent systems. Compared to static ETMs, dynamic ETMs include an additional internal dynamic variable. For example, by introducing a clock variable, the dynamic ETM in [19] guarantees the existence of a positive minimum interevent time (MIET). This feature is appreciated in the implementation of ETMs on physical platforms since it respects hardware limitations. However, existing static ETMs for distributed secondary control of microgrids cannot guarantee the existence of a positive designable MIET, which motivates our current study.

We investigate the distributed event-triggered secondary control of dc microgrids by proposing a distributed dynamic ETM that guarantees a positive designbale MIET. For each converter, a distributed ETC law, based on a distributed voltage observer, is designed, where only output currents of its neighboring converters on the communication graph are needed. To reduce the communication burden, a distributed dynamic ETM is designed by introducing an additional dynamic variable. The resulting closed-loop system dynamics are shown to be asymptotically stable, which implies that the proportional current sharing and global voltage regulation are simultaneously achieved. The main contributions of this article are summarized as follows.

1) The proposed control strategy is fully distributed without requiring any global information of the communication

Manuscript received September 28, 2021; revised December 11, 2021 and February 12, 2022; accepted March 20, 2022. Date of publication March 24, 2022; date of current version May 23, 2022. This work was supported in part by the Department of Navy awards N00014-20-1-2858 and N00014-22-1-2001 issued by the Office of Naval Research, and in part by the National Science Foundation under Grants 1714519 and 1839804. The United States Government has a royalty-free license throughout the world in all copyrightable material contained herein. Recommended for publication by Associate Editor S. Golestan. *(Corresponding author: Yan Wan.)*

Yang-Yang Qian, Abhiram V. P. Premakumar, Yan Wan, and Ali Davoudi are with the Department of Electrical Engineering, University of Texas at Arlington, Arlington, TX 76019 USA (e-mail: yangyang.qian@uta.edu; apv2783@mavs.uta.edu; yan.wan@uta.edu; davoudi@uta.edu).

Zongli Lin is with the Charles L. Brown Department of Electrical and Computer Engineering, University of Virginia, Charlottesville, VA 22904 USA (e-mail: zl5y@virginia.edu).

Yacov A. Shamash is with the Department of Electrical and Computer Engineering, Stony Brook University, Stony Brook, NY 11794 USA (e-mail: yacov.shamash@stonybrook.edu).

Color versions of one or more figures in this article are available at https://doi.org/10.1109/TPEL.2022.3161967.

Digital Object Identifier 10.1109/TPEL.2022.3161967

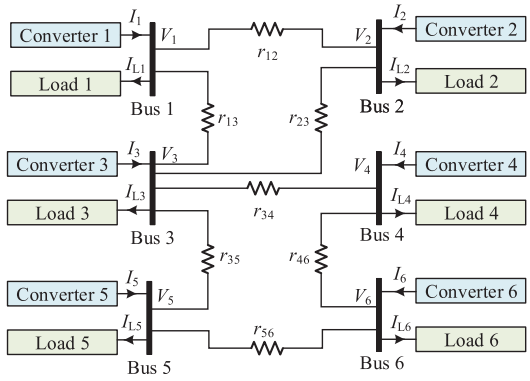

Fig. 1. Schematic of the considered dc microgrid.

graph or the overall closed-loop system dynamics, as opposed to [8].

2) The existence of a positive MIET that can be prespecified is guaranteed under the proposed dynamic ETM, in contrast to the existing static ETMs in [8]–[13]. This implies the exclusion of the Zeno behavior, which is not rigorously proven in [8]–[10].
3) In addition to the exclusion of the Zeno behavior, the adjustment of the positive MIET using the design parameters in the triggering mechanism is discussed, which is not offered in the existing studies [8]–[13].
4) Experimental results in a controller/hardware-in-the-loop (C-HIL) environment validate the proposed control method, including robust performance under load change and communication delay, and performance comparison with the conventional periodic sampling mechanism and the static ETM in [13].

The remainder of this article is organized as follows. Section II presents the notation and the electrical and communication networks. In Section III, the control objectives in a dc microgrid are discussed. In Section IV, a distributed dynamic event-triggered control strategy is designed that guarantees the asymptotic stability of the closed-loop system and the existence of an adjustable positive MIET. Experimental validation, in a C-HIL environment, is provided in Section V. Finally, Section VI concludes this article.

II. Preliminaries

A. Notation

Let $\mathbb{N}$ be the set of all nonnegative integers. The superscript T stands for the transpose. The symbol $\mathbf{1}_N$ represents the N-dimensional column vector with all elements being 1. For a symmetric matrix A, $A > 0$ means that A is positive definite, and $\lambda_{\min}(A)$ denotes its minimal eigenvalue. For a function $f(t) : \mathbb{R} \to \mathbb{R}$, let the left limit and right limit at time t be denoted as $f(t^-)$ and $f(t^+)$, respectively.

B. Electrical Network

The schematic of a dc microgrid is given in Fig. 1. Each node has a dc–dc buck converter and a constant current load. Herein, we consider dc–dc buck converters as microgrid building blocks, which is in line with the majority of microgrid control-themed literature (e.g., [10], [13]). Nevertheless, the proposed control approach is universal, and can be seamlessly applied to dc microgrids with other types of dc–dc converters. The electrical network across all converters is represented by a weighted undirected graph $\mathcal{G}_{\mathrm{e}} = (\mathcal{V}, \mathcal{E}_{\mathrm{e}}, \mathcal{W}_{\mathrm{e}})$, where $\mathcal{V} = \{1, 2, \ldots, N\}$ is the node set, $\mathcal{E}_{\mathrm{e}} \subseteq \mathcal{V} \times \mathcal{V}$ is the edge set, and $\mathcal{W}_{\mathrm{e}} \in \mathbb{R}^{N\times N}$ is the adjacent matrix. The adjacent matrix $\mathcal{W}_{\mathrm{e}}$ is defined as $\mathcal{W}_{\mathrm{e}} = [w_{ij}]$, where $w_{ii} = 0$, $w_{ij} > 0$, if $(j, i) \in \mathcal{E}_{\mathrm{e}}$, and $w_{ij} = 0$, otherwise. In graph $\mathcal{G}_{\mathrm{e}}$, each node is a converter and each edge is a line connecting converters. If there exists a line connecting converter j to converter i, for $i \neq j$, then $(j, i) \in \mathcal{E}_{\mathrm{e}}$ is an edge and the weight of edge (j, i) is the line conductance $w_{ij} = 1/r_{ij}$, with r_{ij} being the line resistance. Let $\mathcal{N}_i^{\mathrm{e}} = \{j : (j, i) \in \mathcal{E}_{\mathrm{e}}\}$ be the set of converters that are electrically connected to converter i. The Laplacian matrix of graph $\mathcal{G}_{\mathrm{e}}$ is defined as $L_{\mathrm{e}} = [l_{ij}^{\mathrm{e}}] \in \mathbb{R}^{N\times N}$, where $l_{ii}^{\mathrm{e}} = \sum_{j\in\mathcal{N}_i^{\mathrm{e}}} w_{ij}$ and $l_{ij}^{\mathrm{e}} = -w_{ij}$, for $i \neq j$. The Laplacian matrix L_{e} is the same as the admittance matrix.

Let V_i, I_i, and $I_{\mathrm{L}i}$ be the bus voltage, the output current, and the load current, for converter i, $i = 1, 2, \ldots, N$. Then, by applying the Kirchhoff's current law (KCL)

$$I_i(t) - I_{\mathrm{L}i} = \sum_{j\in\mathcal{N}_i^{\mathrm{e}}} w_{ij}\left(V_i(t) - V_j(t)\right) \tag{1}$$

for $i = 1, 2, \ldots, N$. Let $I(t) = [I_1(t), I_2(t), \ldots, I_N(t)]^{\mathrm{T}}$, $V(t) = [V_1(t), V_2(t), \ldots, V_{\mathrm{n}}(t)]^{\mathrm{T}}$, and $I_{\mathrm{L}} = [I_{\mathrm{L}1}, I_{\mathrm{L}2}, \ldots, I_{\mathrm{L}N}]^{\mathrm{T}}$. The resistance network of the dc microgrid gives

$$I(t) - I_{\mathrm{L}} = L_{\mathrm{e}}V(t). \tag{2}$$

C. Communication Network

The communication network among converters is represented by a weighted undirected graph $\mathcal{G}_{\mathrm{c}} = (\mathcal{V}, \mathcal{E}_{\mathrm{c}}, \mathcal{A}_{\mathrm{c}})$, where $\mathcal{V}$ is the node set defined in graph $\mathcal{G}_{\mathrm{e}}$, $\mathcal{E}_{\mathrm{c}} \subseteq \mathcal{V} \times \mathcal{V}$ is the edge set, and $\mathcal{A}_{\mathrm{c}} = [a_{ij}] \in \mathbb{R}^{N\times N}$ is the adjacent matrix. The adjacent matrix $\mathcal{A}_{\mathrm{c}}$ is defined as $\mathcal{A}_{\mathrm{c}} = [a_{ij}]$, where $a_{ii} = 0$, $a_{ij} > 0$, if $(j, i) \in \mathcal{E}_{\mathrm{c}}$, and $a_{ij} = 0$, otherwise. In graph $\mathcal{G}_{\mathrm{c}}$, each node is a converter and each edge is a communication link. If there exists a communication link connecting converter j to i, for $i \neq j$, then $(j, i) \in \mathcal{E}_{\mathrm{c}}$ is an edge and the communication weight of edge (j, i) is $a_{ij} > 0$. Let $\mathcal{N}_i^{\mathrm{c}} = \{j : (j, i) \in \mathcal{E}_{\mathrm{c}}\}$ be the set of neighbors of converter i, that can communicate with converter i. The Laplacian matrix of graph $\mathcal{G}_{\mathrm{c}}$ is defined as $L_{\mathrm{c}} = [l_{ij}^{c}] \in \mathbb{R}^{N\times N}$, where $l_{ii}^{\mathrm{c}} = \sum_{j\in\mathcal{N}_i^{\mathrm{c}}} a_{ij}$, and $l_{ij}^{\mathrm{c}} = -a_{ij}$, for $i \neq j$. Note that the topology of the communication network is not necessarily the same as that of the underlying electrical network. The relation between these two network topologies is to be specified later.

III. Control Objectives and Assumptions

The control objectives in a dc microgrid are the proportional load sharing and the global voltage regulation. Proportional current sharing is said to be achieved if, in the steady state, the overall load current is proportionally shared among converters

according to their current ratings, that is,

$$\lim_{t\to\infty}\left(\frac{I_i(t)}{I_{ci}}-\frac{I_j(t)}{I_{cj}}\right)=0, \text{ for all } i,j\in\mathcal{V} \tag{3}$$

where $I_{ci}>0$ and $I_{cj}>0$ are, respectively, the current ratings of converters i and j.

Global voltage regulation is achieved if, in the steady state, the global average voltage across the microgrid distribution line is regulated to the nominal voltage $V_{\rm n}$, that is,

$$\lim_{t\to\infty}\bar{V}(t)\triangleq\lim_{t\to\infty}\frac{1}{N}\sum_{i=1}^{N}V_i(t)=V_{\rm n}. \tag{4}$$

$I_i(t)/I_{ci}$ is the so-called per-unit output current for converter i. The global average voltage $\bar{V}(t)$, which is used in the control laws, is not available to every converter. In this case, a voltage observer will be constructed for each converter to locally estimate $\bar{V}(t)$.

To achieve these two control objectives, we make the following assumptions.

Assumption 1: The graphs $\mathcal{G}_{\rm e}$ and $\mathcal{G}_{\rm c}$ are undirected and connected.

Assumption 2: The Laplacian matrices associated with graphs $\mathcal{G}_e$ and $\mathcal{G}_{\rm c}$ are commutative, that is, $L_{\rm e}L_{\rm c}=L_{\rm c}L_{\rm e}$.

Note that the communication weights $a_{ij}, i,j\in\mathcal{V}$ can be designed such that Assumption 2 is satisfied. To guarantee $L_{\rm e}L_{\rm c}=L_{\rm c}L_{\rm e}$ in Assumption 2, one sufficient condition is $L_{\rm c}=\mu L_{\rm e}$, where μ is a positive constant. The relation $L_{\rm c}=\mu L_{\rm e}$ holds, if the following conditions are simultaneously guaranteed: 1) The graphs $\mathcal{G}_{\rm e}$ and $\mathcal{G}_c$ have the same topology; and 2) the communication weight a_{ij} is chosen as $a_{ij}=\mu w_{ij}$, if there exists a communication link between converters i and j.

Under Assumption 2, the topologies of graphs $\mathcal{G}_{\rm e}$ and $\mathcal{G}_{\rm c}$ are not necessarily the same. To illustrate this, consider the case when the graphs $\mathcal{G}_{\rm e}$ and $\mathcal{G}_{\rm c}$ have different topologies and their Laplacian matrices are given by

$$L_{\rm e}=\begin{bmatrix}2&-1&-1\\-1&2&-1\\-1&-1&2\end{bmatrix}, L_{\rm c}=\begin{bmatrix}2&-1&-1\\-1&1&0\\-1&0&1\end{bmatrix} \tag{5}$$

where the unit of the elements in $L_{\rm e}$ is Ω^{-1}. Then, there holds

$$L_{\rm e}L_{\rm c}=L_{\rm c}L_{\rm e}=\begin{bmatrix}6&-3&-3\\-3&3&0\\-3&0&3\end{bmatrix}. \tag{6}$$

This indicates that Assumption 2 could be satisfied even when the topologies of graphs $\mathcal{G}_{\rm e}$ and $\mathcal{G}_{\rm c}$ are different.

Under Assumptions 1 and 2, the Laplacian matrices $L_{\rm e}$ and $L_{\rm c}$ have the following property, which is needed in our stability analysis.

Lemma 1: Given the two graphs $\mathcal{G}_{\rm e}$ and $\mathcal{G}_{\rm c}$ under Assumptions 1 and 2, their Laplacian matrices $L_{\rm e}$ and $L_{\rm c}$ satisfy

$$L_{\rm e}=L_{\rm c}Q \tag{7}$$

where Q is a positive-definite matrix.

Proof: See Appendix A. ■

IV. Distributed Dynamic Event-Triggering Mechanism

A distributed dynamic ETC strategy will achieve the control objectives of a dc microgrid using a distributed ETC law and a distributed dynamic ETM. A uniform positive MIET is provided for each converter. The stability of the resulting closed-loop system under the proposed ETC strategy is analyzed. Finally, adjusting the positive MIET using the design parameters in the triggering mechanism is discussed.

A. Event-Triggered Control Law

Let $\hat{I}_i(t)$ be the latest sampled output current of converter i at time t. Then, $\hat{I}_i(t)$ can be expressed as

$$\hat{I}_i(t)=I_i(t_k^i), t\in[t_k^i,t_{k+1}^i) \tag{8}$$

where t_k^i is the kth event time of converter i, for $k\in\mathbb{N}$. Inspired by [13], a distributed ETC law is designed as

$$\begin{aligned}\dot{V}_i^{\rm ref}(t)=&-K_I\sum_{j\in\mathcal{N}_i^{\rm c}}a_{ij}\left(\frac{\hat{I}_i(t)}{I_{ci}}-\frac{\hat{I}_j(t)}{I_{cj}}\right)\\&-K_V\left(\bar{V}_i(t)-V_{\rm n}\right)\end{aligned} \tag{9}$$

where $K_I>0$ and $K_V>0$ are the controller gains; $V_i^{\rm ref}(t)$ is the reference voltage; and $\bar{V}_i(t)$ is the observer state in converter i to estimate the global average voltage $\bar{V}(t)=(1/N)\sum_{i=1}^{N}V_i(t)$. The observer state $\bar{V}_i(t)$ is generated by the following distributed voltage observer:

$$\bar{V}_i(t)=V_i(t)+K\int_0^t\sum_{j\in\mathcal{N}_i^{\rm c}}a_{ij}\left(\frac{\hat{I}_i(\tau)}{I_{ci}}-\frac{\hat{I}_j(\tau)}{I_{cj}}\right)d\tau. \tag{10}$$

$K>K_I$ is the observer gain. Note that the observer (10) provides an auxiliary variable $\bar{V}_i(t)$ for the design of controller (9). As in [10], [13], and [22], it is reasonable to neglect the converter dynamics and assume that $V_i(t)=V_i^{\rm ref}(t)$. Then, it follows from (9) that the bus voltage $V_i(t)$ is updated by

$$\begin{aligned}\dot{V}_i(t)=&-K_I\sum_{j\in\mathcal{N}_i^{\rm c}}a_{ij}\left(\frac{\hat{I}_i(t)}{I_{ci}}-\frac{\hat{I}_j(t)}{I_{cj}}\right)\\&-K_V\left(\bar{V}_i(t)-V_{\rm n}\right).\end{aligned} \tag{11}$$

To implement the distributed ETC law (9) with the distributed voltage observer (10), only the per-unit output current information, i.e., $\hat{I}_i(t)/I_{ci}$, $i\in\mathcal{V}$, is exchanged among converters through the communication network. Specifically, each converter broadcasts its per-unit output current, $\hat{I}_i(t)/I_{ci}$, at event times to its neighbors on graph $\mathcal{G}_{\rm c}$.

Differently from the conventional distributed voltage observer in [5] and [23], the distributed voltage observer (11) depends on the per-unit output currents of converter i and its neighbors on graph $\mathcal{G}_{\rm c}$, instead of both their per-unit output currents and voltage observer states. This way, less information is exchanged among converters to implement the proposed distributed control law in comparison with those in [5] and [23]. In addition, the distributed voltage observer (10) has an additional degree of freedom compared with the distributed voltage observer in [13]

of the form

$$\bar{V}_i(t)=V_i(t)+(K_I+K_V)\int_0^t\sum_{j\in\mathcal{N}_i^{\rm c}}a_{ij}\left(\frac{\hat{I}_i(\tau)}{I_{{\rm c}i}}-\frac{\hat{I}_j(\tau)}{I_{{\rm c}j}}\right)d\tau. \tag{12}$$

The observer gain in the voltage observer (12) is fixed once the controller gains K_I and K_V are determined. By contrast, the observer gain K in (10) can be designed. As such, the performance of the voltage observer (10) can be adjusted by a proper observer gain K. While the distributed ETC law (9) is inspired by [13], this article designs a new distributed ETM that guarantees a positive MIET.

B. Dynamic Event-Triggering Mechanism

A distributed dynamic ETM decides when each converter broadcasts its information. To develop the ETM, define the measurement error for each converter i as

$$e_i(t)=\frac{\hat{I}_i(t)}{I_{{\rm c}i}}-\frac{I_i(t)}{I_{{\rm c}i}}, t\in[t_k^i,t_{k+1}^i). \tag{13}$$

Further, define a dynamic trigger variable updated by

$$\begin{cases}\dot{\eta}_i(t)=\begin{cases}\min\{\varpi_i(t),0\}-\alpha_i, & \text{if } e_i(t)\neq 0\\ -\alpha_i, & \text{if } e_i(t)=0\end{cases}\\ \qquad\text{for } t\in(t_k^i,t_{k+1}^i)\\ \eta_i(t^+)=\beta_i, \text{ for } t=t_k^i\end{cases} \tag{14}$$

with

$$\begin{aligned}\varpi_i(t)\triangleq\ &\frac{\sigma_i}{I_{{\rm c}i}}K_I\left(\lambda_{\min}(Q)-3\kappa d_i\right)\frac{1}{e_i^2(t)}\\ &\times\left[\sum_{j\in\mathcal{N}_i^{\rm c}}a_{ij}\left(\frac{\hat{I}_i(t)}{I_{{\rm c}i}}-\frac{\hat{I}_j(t)}{I_{{\rm c}j}}\right)\right]^2\\ &+\frac{2\sigma_i}{I_{{\rm c}i}}K_V\left(\frac{K_V\lambda_{\min}(Q)}{K-K_I}-2\kappa d_i\right)\frac{1}{e_i^2(t)}\\ &\times\left(\bar{V}_i(t)-V_{\rm n}\right)^2\\ &-\frac{2}{\kappa I_{{\rm c}i}}\left(K_I+K_V\right)d_i\left(1+\eta_i^2(t)\right)\end{aligned} \tag{15}$$

where $Q>0$ is given in (7), $d_i\triangleq\sum_{j=1}^N w_{ij}$ is the degree of converter i on graph $\mathcal{G}_{\rm e}$, and α_i, β_i, σ_i, and κ are the design parameters satisfying $\alpha_i>0, \beta_i>0, 0<\sigma_i<1$, and $0<\kappa<\kappa_{\max}\triangleq\min\{\lambda_{\min}(Q)/(3\max_{i\in\mathcal{V}}d_i), K_V\lambda_{\min}(Q)/[2(K-K_I)\max_{i\in\mathcal{V}}d_i]\}$, respectively. Let $\{t_k^i:k\in\mathbb{N}\}$ be the sequence of event times for converter i. Then, to determine the time sequence $\{t_k^i:k\in\mathbb{N}\}$, a distributed dynamic ETM is designed as

$$t_{k+1}^i=\inf\{t>t_k^i\mid\eta_i(t)\leq 0\} \tag{16}$$

for $k\in\mathbb{N}$, where t_0^i is arbitrary. In the ETM (16), the dynamics of the trigger variable $\eta_i(t)$ depend on the triggered per-unit output current information of converter i and its neighbors on graph $\mathcal{G}_{\rm c}$, that is, $\hat{I}_i(t)/I_{{\rm c}i}$ and $\hat{I}_j(t)/I_{{\rm c}j}$, $j\in\mathcal{N}_i^{\rm c}$. In this sense, the ETM (16) is considered *distributed*. Moreover, the ETM (16) is considered *dynamic* due to the presence of the additional internal dynamic variable $\eta_i(t)$.

The design idea of the ETM (16) is to make $\eta_i(t)$ decrease from β_i to 0 during the time-interval (t_k^i,t_{k+1}^i), and to reset $\eta_i(t)$ from 0 to β_i at each event time t_k^i. Clearly, $0\leq\eta_i(t)\leq\beta_i$ holds for all $t\geq 0$. It should be pointed out that $\varpi_i(t)$ in (15) is designed to make the closed-loop system stable. To guarantee the feasibility of the ETM (16), the Zeno behavior, an infinite number of events occurring in a finite time-interval, is excluded for each converter, as shown below. Note that the Zeno behavior occurs for converter i if there exists a finite accumulation time $T_i>0$ by which an infinite number of events have occurred, that is, $\lim_{k\to\infty}t_k^i=T_i$.

Theorem 1: Under the distributed dynamic ETM (16), the interevent times $t_{k+1}^i-t_k^i, k\in\mathbb{N}$, for converter i, have a uniform positive lower bound

$$\begin{aligned}\tau_i=\sqrt{\frac{\kappa}{\alpha_i\gamma_i}}\Bigg[&\arctan\left(\sqrt{\frac{\gamma_i}{\kappa\alpha_i}}\left(\beta_i+1\right)\right)\\ &-\arctan\left(\sqrt{\frac{\gamma_i}{\kappa\alpha_i}}\right)\Bigg]>0\end{aligned} \tag{17}$$

where $\gamma_i\triangleq(2/I_{{\rm c}i})(K_I+K_V)d_i$. This implies that the Zeno behavior is excluded for each converter.

Proof: See Appendix B. ■

The lower-bound τ_i given by (17) is called the MIET of converter i. The MIET τ_i is uniform in k and independent of the state information, and can be prespecified by the designer. By Theorem 1, the distributed dynamic ETM (16) can be equivalently expressed as

$$t_{k+1}^i=\inf\{t\geq t_k^i+\tau_i\mid\eta_i(t)\leq 0\}. \tag{18}$$

The positive MIET τ_i is explicitly enforced. This allows the event-triggering condition $\eta_i(t)\leq 0$ to be checked after the dwell time τ_i when $t=t_k^i$. Thus, the ETM (18) can be implemented as follows. During the time-interval $[t_k^i+\tau_i,\infty)$, the event-triggering condition $\eta_i(t)\leq 0$ is checked, and an event is triggered if $\eta_i(t)\leq 0$ holds. At each event time t_k^i, $k\in\mathbb{N}$, converter i resets the trigger variable $\eta_i(t)$ to the maximum value β_i, updates the triggered per-unit current $\hat{I}_i(t)/I_{{\rm c}i}$ with the real-time one $I_i(t)/I_{{\rm c}i}$, and broadcasts the real-time per-unit output current $I_i(t)/I_{{\rm c}i}$ to each neighbor on graph $\mathcal{G}_{\rm c}$. In addition, converter i updates the triggered per-unit output current $\hat{I}_j(t)/I_{{\rm c}j}$ with $I_j(t)/I_{{\rm c}j}$, once $I_j(t)/I_{{\rm c}j}$ is received from its neighboring converter j, $j\in\mathcal{N}_i^{\rm c}$.

C. Closed-Loop System Stability

The stability analysis is presented for the closed-loop system under the distributed ETC law (9) and the distributed dynamic ETM (18).

Define the following error variables:

$$\delta_{Ii}(t)=\sum_{j\in\mathcal{N}_i^{\rm c}}a_{ij}\left(\frac{I_i(t)}{I_{{\rm c}i}}-\frac{I_j(t)}{I_{{\rm c}j}}\right) \tag{19a}$$

$$\hat{\delta}_{Ii}(t)=\sum_{j\in\mathcal{N}_i^{\rm c}}a_{ij}\left(\frac{\hat{I}_i(t)}{I_{{\rm c}i}}-\frac{\hat{I}_j(t)}{I_{{\rm c}j}}\right) \tag{19b}$$

$$\delta_V(t)=\bar{V}(t)-V_{\rm n} \tag{19c}$$

$$\bar{\delta}_{Vi}(t)=\bar{V}_i(t)-V_{\rm n}. \tag{19d}$$

Let $\delta_I = [\delta_{I1}, \delta_{I2}, \ldots, \delta_{IN}]^{\mathrm{T}}$, $\hat{\delta}_I = [\hat{\delta}_{I1}, \hat{\delta}_{I2}, \ldots, \hat{\delta}_{IN}]^{\mathrm{T}}$, $\delta_V = [\delta_{V1}, \delta_{V2}, \ldots, \delta_{VN}]^{\mathrm{T}}$, $\bar{\delta}_V = [\bar{\delta}_{V1}, \bar{\delta}_{V2}, \ldots, \bar{\delta}_{VN}]^{\mathrm{T}}$, $\hat{I} = [\hat{I}_1, \hat{I}_2, \ldots, \hat{I}_N]^{\mathrm{T}}$, $e = [e_1, e_2, \ldots, e_N]^{\mathrm{T}}$, and $I_{\mathrm{c}} = \mathrm{diag}\{I_{\mathrm{c}1}, I_{\mathrm{c}2}, \ldots, I_{\mathrm{c}N}\}$. Then, one has

$$e(t) = I_{\mathrm{c}}^{-1}\hat{I}(t) - I_{\mathrm{c}}^{-1}I(t) \tag{20}$$

and

$$\delta_I(t) = L_{\mathrm{c}}I_{\mathrm{c}}^{-1}I(t) \tag{21a}$$

$$\hat{\delta}_I(t) = L_{\mathrm{c}}I_{\mathrm{c}}^{-1}\hat{I}(t) = \delta_I(t) + L_{\mathrm{c}}e(t) \tag{21b}$$

$$\delta_V(t) = \frac{1}{N}\mathbf{1}_N^{\mathrm{T}}V(t) - V_{\mathrm{n}} \tag{21c}$$

$$\bar{\delta}_V(t) = V(t) + K\int_0^t \hat{\delta}_I(\tau)d\tau - V_{\mathrm{n}}\mathbf{1}_N. \tag{21d}$$

Under Assumption 1, the null space of L_{c} is span$\{\mathbf{1}_N\}$ [24]. Then, $\delta_I(t) = L_{\mathrm{c}}I_{\mathrm{c}}^{-1}I(t) = 0$ implies that $I_{\mathrm{c}}^{-1}I(t) = \alpha\mathbf{1}_N$, with α being a real number. Hence, the control objectives of proportional current sharing and global voltage regulation are achieved if $\lim_{t\to\infty}\delta_I(t) = 0$ and $\lim_{t\to\infty}\delta_V(t) = 0$.

From the bus voltage $V_i(t)$ in (11), it follows that

$$\dot{V}(t) = -K_I\hat{\delta}_I(t) - K_V\bar{\delta}_V(t). \tag{22}$$

Combine (2) and (20)–(22), and use $\mathbf{1}_N^{\mathrm{T}}L_{\mathrm{c}} = 0$ to yield

$$\dot{I}(t) = L_{\mathrm{e}}\dot{V}(t) = -K_IL_{\mathrm{e}}\hat{\delta}_I(t) - K_VL_{\mathrm{e}}\bar{\delta}_V(t) \tag{23a}$$

$$\begin{aligned}\dot{\delta}_V(t) &= \frac{1}{N}\mathbf{1}_N^{\mathrm{T}}\dot{V}(t) = -\frac{1}{N}K_V\mathbf{1}_N^{\mathrm{T}}\bar{\delta}_V(t)\\ &= -\frac{1}{N}K_V\left(\mathbf{1}_N^{\mathrm{T}}V(t) - V_{\mathrm{n}}\mathbf{1}_N^{\mathrm{T}}\mathbf{1}_N\right)\\ &= -K_V\delta_V(t)\end{aligned} \tag{23b}$$

$$\begin{aligned}\dot{\bar{\delta}}_V(t) &= \dot{V}(t) + K\hat{\delta}_I(t)\\ &= (K - K_I)\,\hat{\delta}_I(t) - K_V\bar{\delta}_V(t)\end{aligned} \tag{23c}$$

$$\begin{aligned}\dot{e}(t) &= -I_{\mathrm{c}}^{-1}\dot{I}(t)\\ &= K_II_{\mathrm{c}}^{-1}L_{\mathrm{e}}\hat{\delta}_I(t) + K_VI_{\mathrm{c}}^{-1}L_{\mathrm{e}}\bar{\delta}_V(t).\end{aligned} \tag{23d}$$

Let $\{t_l : l \in \mathbb{N}\}$ be the strictly increasing sequence of event times for all converters. Then, the resulting closed-loop system is modeled by an impulsive dynamical system, where the flow dynamics are

$$\dot{I}(t) = -K_IL_{\mathrm{e}}\hat{\delta}_I(t) - K_VL_{\mathrm{e}}\bar{\delta}_V(t) \tag{24a}$$

$$\dot{\delta}_V(t) = -K_V\delta_V(t) \tag{24b}$$

$$\dot{\bar{\delta}}_V(t) = (K - K_I)\,\hat{\delta}_I(t) - K_V\bar{\delta}_V(t) \tag{24c}$$

$$\dot{e}(t) = K_II_{\mathrm{c}}^{-1}L_{\mathrm{e}}\hat{\delta}_I(t) + K_VI_{\mathrm{c}}^{-1}L_{\mathrm{e}}\bar{\delta}_V(t) \tag{24d}$$

$$\dot{\eta}_i(t) = \begin{cases}\min\{\varpi_i(t), 0\} - \alpha_i, & \text{if } e_i(t) \neq 0\\ -\alpha_i, & \text{if } e_i(t) = 0\end{cases} \tag{24e}$$

for $t \neq t_l$, and the jump dynamics, for $t = t_l$, are

$$I(t^+) = I(t^-), \delta_V(t^+) = \delta_V(t^-), \bar{\delta}_V(t^+) = \bar{\delta}_V(t^-) \tag{24f}$$

$$e_i(t^+) = \begin{cases}e_i(t^-), & \text{if } t \neq t_k^i\\ 0, & \text{if } t = t_k^i\end{cases} \tag{24g}$$

$$\eta_i(t^+) = \begin{cases}\eta_i(t^-), & \text{if } t \neq t_k^i\\ \beta_i, & \text{if } t = t_k^i\end{cases} \tag{24h}$$

with $i \in \mathcal{V}$.

In virtue of Lemma 1, we are ready to obtain the following result on the stability of the closed-loop system (24a)–(24h).

Theorem 2: Consider the closed-loop system (24a)–(24h) under Assumptions 1 and 2. If the distributed dynamic ETM (18) is executed, then the error variables $\delta_I(t)$, $\hat{\delta}_I(t)$, $\delta_V(t)$, and $\bar{\delta}_V(t)$ converge to the origin asymptotically, which implies that the control objectives of proportional current sharing and global voltage regulation are simultaneously achieved.

Proof: See Appendix C. ■

Given the line resistances r_{ij}, $i, j \in \mathcal{V}$, in the considered dc microgrid, the communication weights a_{ij}, $i, j \in \mathcal{V}$, can be designed as $a_{ij} = \mu w_{ij} = \mu/r_{ij}$, with μ being any positive constant, such that Assumption 2 is satisfied. In this case, the line resistances affect the performance of the proposed controller (9), as discussed below. In the resulting closed-loop system (24a)–(24h), the dynamics of the output currents vector $I(t)$ depend on the Laplacian matrix L_{e} associated with the electrical network. Recall that the Laplacian matrix L_{e} is defined based on the line resistances in the microgrid. Thus, the line resistances affect the load sharing performance. In addition, the time-derivative of the Lyapunov function $W(t)$, given in the proof of Theorem 2, depends on the Laplacian matrix L_{e}. This indicates that the line resistances also affect the stability of the closed-loop system (24a)–(24h).

D. Adjustment of the Minimum Inter-Event Time

One can adjust the positive MIET τ_i in (17) using proper parameters α_i, β_i, and κ in the triggering mechanism. Consider the following three cases.

Case 1: α_i is varied. The partial derivative of τ_i with respect to α_i is given by

$$\begin{aligned}\frac{\partial\tau_i}{\partial\alpha_i} =& -\frac{1}{2\alpha_i^2}\sqrt{\frac{\kappa\alpha_i}{\gamma_i}}\\ &\times\left[\arctan\left(\sqrt{\frac{\gamma_i}{\kappa\alpha_i}}\,(\beta_i+1)\right) - \arctan\left(\sqrt{\frac{\gamma_i}{\kappa\alpha_i}}\right)\right]\\ &+\frac{1}{2\alpha_i^2}\left[\frac{1}{1+\frac{\gamma_i}{\kappa\alpha_i}} - \frac{\beta_i+1}{1+\frac{\gamma_i}{\kappa\alpha_i}(\beta_i+1)^2}\right].\end{aligned} \tag{25}$$

To compute the first term in the right side of (25), consider the continuous function $f(x) = \arctan(x)$ on the interval $(\sqrt{\gamma_i/(\kappa\alpha_i)}, \sqrt{\gamma_i/(\kappa\alpha_i)}(\beta_i+1))$. By the mean-value theorem, there exists a point $p_i \in (\sqrt{\gamma_i/(\kappa\alpha_i)}, \sqrt{\gamma_i/(\kappa\alpha_i)}(\beta_i+1))$ such that

$$\begin{aligned}&\arctan\left(\sqrt{\frac{\gamma_i}{\kappa\alpha_i}}\,(\beta_i+1)\right) - \arctan\left(\sqrt{\frac{\gamma_i}{\kappa\alpha_i}}\right)\\ &= f'(p_i)\beta_i\sqrt{\frac{\gamma_i}{\kappa\alpha_i}}.\end{aligned} \tag{26}$$

Since $p_i \in (\sqrt{\gamma_i/(\kappa\alpha_i)}, \sqrt{\gamma_i/(\kappa\alpha_i)}(\beta_i+1))$, there holds

$$f'(p_i) = \frac{1}{1+p_i^2} \geq \frac{1}{1+\frac{\gamma_i}{\kappa\alpha_i}(\beta_i+1)^2}. \tag{27}$$

Then, it follows from (26) and (27) that

$$\arctan\left(\sqrt{\frac{\gamma_i}{\kappa\alpha_i}}(\beta_i+1)\right) - \arctan\left(\sqrt{\frac{\gamma_i}{\kappa\alpha_i}}\right) \geq \sqrt{\frac{\gamma_i}{\kappa\alpha_i}}\frac{\beta_i}{1+\frac{\gamma_i}{\kappa\alpha_i}(\beta_i+1)^2}. \tag{28}$$

In addition, one has

$$\frac{1}{1+\frac{\gamma_i}{\kappa\alpha_i}} - \frac{\beta_i+1}{1+\frac{\gamma_i}{\kappa\alpha_i}(\beta_i+1)^2} = \frac{\beta_i\left[\frac{\gamma_i}{\kappa\alpha_i}(\beta_i+1)-1\right]}{\left(1+\frac{\gamma_i}{\kappa\alpha_i}\right)\left[1+\frac{\gamma_i}{\kappa\alpha_i}(\beta_i+1)^2\right]}. \tag{29}$$

Substituting (28) and (29) into (25) yields

$$\begin{aligned}\frac{\partial\tau_i}{\partial\alpha_i} &\leq -\frac{1}{2\alpha_i^2}\frac{\beta_i}{1+\frac{\gamma_i}{\kappa\alpha_i}(\beta_i+1)^2} + \frac{1}{2\alpha_i^2} \times \frac{\beta_i\left[\frac{\gamma_i}{\kappa\alpha_i}(\beta_i+1)-1\right]}{\left(1+\frac{\gamma_i}{\kappa\alpha_i}\right)\left[1+\frac{\gamma_i}{\kappa\alpha_i}(\beta_i+1)^2\right]} \\ &= -\frac{\beta_i}{2\alpha_i^2}\frac{2-\frac{\gamma_i}{\kappa\alpha_i}\beta_i}{\left(1+\frac{\gamma_i}{\kappa\alpha_i}\right)\left[1+\frac{\gamma_i}{\kappa\alpha_i}(\beta_i+1)^2\right]}.\end{aligned} \tag{30}$$

This implies that $\partial\tau_i/\partial\alpha_i < 0$ if $\gamma_i\beta_i < 2\kappa\alpha_i$. Thus, τ_i is a decreasing function of α_i if $\gamma_i\beta_i < 2\kappa\alpha_i$.

Case 2: β_i is varied. The partial derivative of τ_i with respect to β_i is given by

$$\frac{\partial\tau_i}{\partial\beta_i} = \frac{1}{\alpha_i+\frac{\gamma_i}{\kappa}(\beta_i+1)^2} > 0. \tag{31}$$

Thus, τ_i is an increasing function of β_i.

Case 3: κ is varied. The partial derivative of τ_i with respect to κ is given by

$$\begin{aligned}\frac{\partial\tau_i}{\partial\kappa} &= \frac{1}{2}\sqrt{\frac{1}{\kappa\alpha_i\gamma_i}} \times \left[\arctan\left(\sqrt{\frac{\gamma_i}{\kappa\alpha_i}}(\beta_i+1)\right) - \arctan\left(\sqrt{\frac{\gamma_i}{\kappa\alpha_i}}\right)\right] \\ &\quad + \frac{1}{2\kappa\alpha_i}\left[\frac{1}{1+\frac{\gamma_i}{\kappa\alpha_i}} - \frac{\beta_i+1}{1+\frac{\gamma_i}{\kappa\alpha_i}(\beta_i+1)^2}\right].\end{aligned} \tag{32}$$

Substituting (28) and (29) into (32) yields

$$\begin{aligned}\frac{\partial\tau_i}{\partial\kappa} &\geq \frac{1}{2\kappa\alpha_i}\frac{\beta_i}{1+\frac{\gamma_i}{\kappa\alpha_i}(\beta_i+1)^2} + \frac{1}{2\kappa\alpha_i}\frac{\beta_i\left[\frac{\gamma_i}{\kappa\alpha_i}(\beta_i+1)-1\right]}{\left(1+\frac{\gamma_i}{\kappa\alpha_i}\right)\left[1+\frac{\gamma_i}{\kappa\alpha_i}(\beta_i+1)^2\right]} \\ &= \frac{\beta_i}{2\kappa\alpha_i}\frac{\frac{\gamma_i}{\kappa\alpha_i}(\beta_i+2)}{\left(1+\frac{\gamma_i}{\kappa\alpha_i}\right)\left[1+\frac{\gamma_i}{\kappa\alpha_i}(\beta_i+1)^2\right]} \\ &> 0.\end{aligned} \tag{33}$$

Thus, τ_i is an increasing function of κ.

In summary, the relation between the MIET τ_i and the design parameters α_i, β_i, and κ is given as follows.

1) τ_i is a decreasing function of α_i if $\gamma_i\beta_i < 2\kappa\alpha_i$.
2) τ_i is an increasing function of β_i.
3) τ_i is an increasing function ofκ.

Therefore, the MIET τ_i can be made larger by increasing the parameters β_i and κ, or by decreasing the parameter α_i, as long as $\gamma_i\beta_i < 2\kappa\alpha_i$.

E. Parameter Design Guideline

The parameter design is summarized as follows.

1) The proportional and integral gains in the inner voltage and current control loops are chosen such that the bus voltage at each converter can quickly track its reference voltage provided by the proposed controller.
2) The controller gains $K_I > 0$ and $K_V > 0$ are chosen to achieve the desired control performance in the proportional current sharing and global voltage regulation.
3) The observer gain $K > K_I$ is chosen to make the observer state $\bar{V}_i(t)$ quickly estimate the global average voltage $\bar{V}(t)$.
4) The trigger parameters κ, α_i, β_i, and σ_i are chosen to adjust the MIET τ_i as discussed in Section IV-D.

V. Controller/Hardware-in-The-Loop Validation

A. Microgrid Testbed

The proposed distributed dynamic ETC strategy is validated on a dc microgrid testbed, with its schematic shown in Fig. 1, that is deployed in a C-HIL environment (Fig. 2). This testbed has six buck converters with constant current loads. The example of one converter is shown in Fig. 3. The proposed control strategy is implemented in dSPACE control board (DS1202). Cascaded voltage and current control loops, using proportional–integral (PI) controllers [25], are adopted for local converter control.

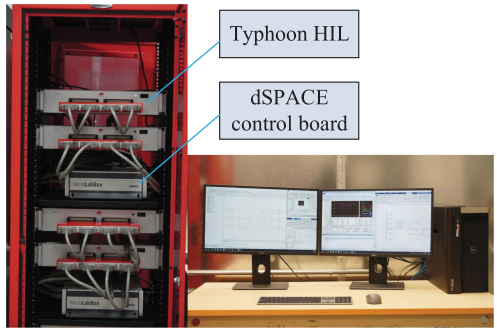

Fig. 2. C-HIL setup, where the physical system is emulated in Typhoon HIL604 and the cyber domain is represented in dSPACE DS1202 control board.

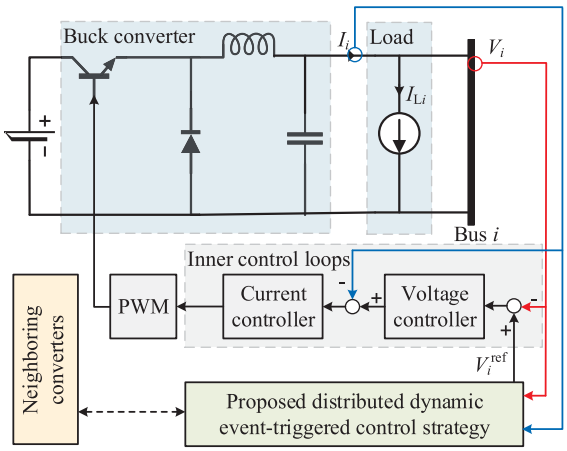

Fig. 3. Structure of the ith buck converter.

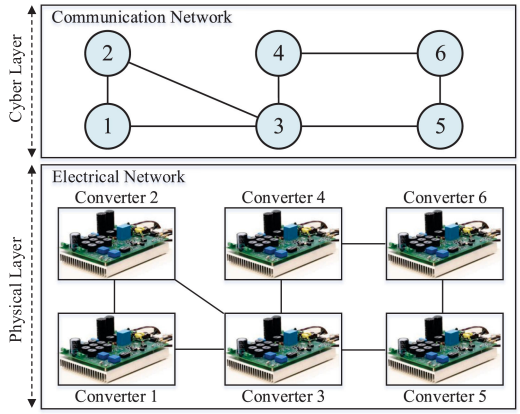

Fig. 4. Conceptual topologies of the electrical and communication networks, respectively, in the physical and cyber layers.

TABLE I
MICROGRID PARAMETERS

Parameter	Symbol	Value	Unit
Voltage source	V_s	100	V
Internal resistance (source)	r_s	0.1	Ω
Converter output inductor	L	1.8	mH
Converter output capacitor	C	2.2	mF
Converter output inductor ESR	r_L	520	mΩ
Converter output capacitor ESR	r_C	50	mΩ
Switching frequency	f_{sw}	20	kHz
Nominal voltage	V_n	48	V
Line resistances	r_{12}, r_{34}, r_{56}	0.5	Ω
	$r_{13}, r_{23}, r_{35}, r_{46}$	0.25	Ω

Each dc source in Fig. 3 is modeled as a voltage source in series with an internal resistance. The microgrid parameters, which are determined based on those in [10], [13], and [26], are shown in Table I.

To satisfy Assumption 2, let the communication network have the same topology as that of the electrical network, and choose the communication weight $a_{ij} = w_{ij} = 1/r_{ij}$, if converter i and converter j are connected by a communication link, for $i, j =$ 1, 2, …, 6. The communication network among converters is represented by the graph in Fig. 4. The adjacent matrices $\mathcal{W}_e$ and $\mathcal{A}_c$ associated with the electrical and communication networks are given by

$$\mathcal{W}_e = \mathcal{A}_c = \begin{bmatrix} 0 & 2 & 4 & 0 & 0 & 0 \\ 2 & 0 & 4 & 0 & 0 & 0 \\ 4 & 4 & 0 & 2 & 4 & 0 \\ 0 & 0 & 2 & 0 & 0 & 4 \\ 0 & 0 & 4 & 0 & 0 & 2 \\ 0 & 0 & 0 & 4 & 2 & 0 \end{bmatrix}. \tag{34}$$

The following parameters are considered. Rated currents I_{ci}, $i = 1, 2, \ldots, 6$ are 10, 5, 5, 10, 6, and 8 A, respectively. Initial load currents I_{Li}, $i = 1, 2, \ldots, 6$ are 2, 4, 3, 5, 3, and 5 A, respectively. The proportional and integral gains in the voltage controller are 0.5 and 0.1, respectively. The proportional and integral gains in the current controller are 0.5 and 0.1, respectively. The controller gains in (9) are $K_I = 3$ and $K_V = 6$. The observer gain in (10) is $K = 9$. Trigger parameters are $\kappa = 0.023$, $\alpha_i = 0.01 + 0.001 \times i$, $\beta_i = 5.0 + 0.2 \times i$, and $\sigma_i = 0.9 + 0.01 \times i$, for $i = 1, 2, \ldots, 6$. It can be verified that $\kappa < \kappa_{\max} = 0.0238$.

TABLE II
LOAD SETTINGS

Time period (s)	Load current (A)					
	I_{L1}	I_{L2}	I_{L3}	I_{L4}	I_{L5}	I_{L6}
$[0, 10)$	2	4	3	5	3	5
$[10, 30)$	3	2	4	4	4	4
$[30, 50]$	4	3	5	6	5	6

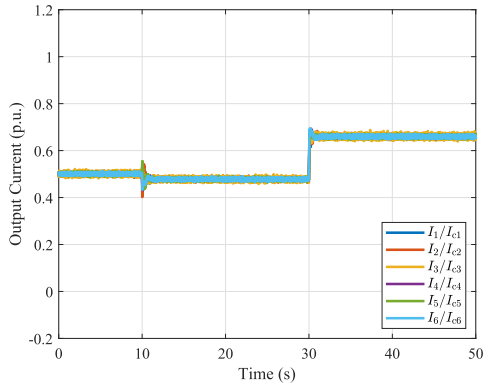

Fig. 5. Converter output currents in p.u., I_i/I_{ci}, $i = 1, 2, \ldots, 6$.

B. Experimental Results

1) Load Change: Consider the case of various load conditions listed in Table II. The load changes occur at $t = 10$ s and $t = 30$ s. Specifically, the overall load current decreases from 22 to 21 A at $t = 10$ s, and increases from 21 to 29 A at $t = 30$ s. Fig. 5 shows converter output currents in per unit (p.u.), that is, $I_i(t)/I_{ci}$, $i = 1, 2, \ldots, 6$. Fig. 6 shows the converters' bus voltages, that is, $V_i(t)$, $i = 1, 2, \ldots, 6$, and the global average voltage $\bar{V}(t)$. In Figs. 5 and 6, it can be seen that the converter output currents and the bus voltages are quickly regulated and

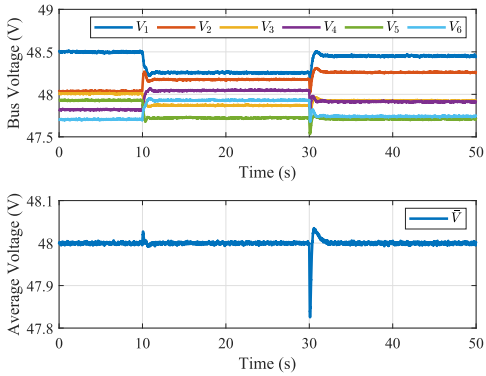

Fig. 6. Bus voltages V_i, $i = 1, 2, \ldots, 6$, and the global average voltage $\bar{V}$.

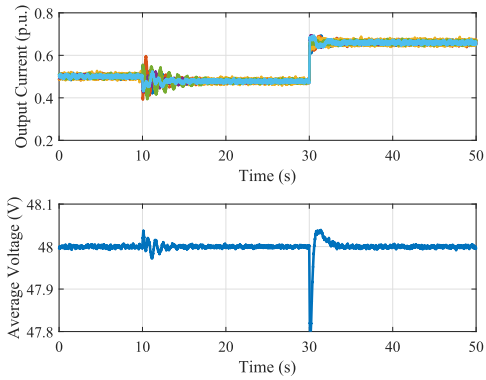

Fig. 7. Experimental results when $K_I = 1$ and $K_V = 2$.

TABLE III
NUMBER OF INFORMATION TRANSMISSIONS FOR EACH CONVERTER UNDER DIFFERENT K_I AND K_V

Parameter setting	Number of information transmissions for converter i					
	$i = 1$	$i = 2$	$i = 3$	$i = 4$	$i = 5$	$i = 6$
$K_I = 3$, $K_V = 6$	3384	8639	38017	2804	5914	3784
$K_I = 1$, $K_V = 2$	1364	3580	16055	1080	2407	1541

the voltage deviation of the bus voltage $V_i(t)$ is within 5% of the nominal voltage V_n, that is, $45.6\ \text{V} < V_i(t) < 50.4\ \text{V}$.

2) Tradeoff in Parameter Design: There exists a tradeoff between the control performance and the communication burden. Specifically, the dynamic response of the control system can be made faster at the cost of a larger number of information transmissions. To illustrate this, consider the parameter setting as in the previous case except that $K_I = 1$ and $K_V = 2$. Then, under the proposed control strategy, the converters' output currents in p.u. and the global average voltage are shown in Fig. 7, and the number of information transmissions for each converter during the time-interval [0,50] s is given in Table III. By comparing Fig. 7 with Figs. 5 and 6, one can observe that the dynamic response becomes faster by increasing K_I and K_V. As a tradeoff, the number of information transmissions for each converter becomes larger, as seen from Table III.

To illustrate the triggering of events (information transmissions), the trigger variable $\eta_1(t)$ of converter 1 is shown in Fig. 8, where $\eta_1(t)$ decreases from β_1 to 0, and is reset to β_1 at event times when $\eta_1(t) = 0$ holds. The observed MIETs for converters $i, i = 1, 2, \ldots, 6$, during the time-interval [15, 20] s, as seen from

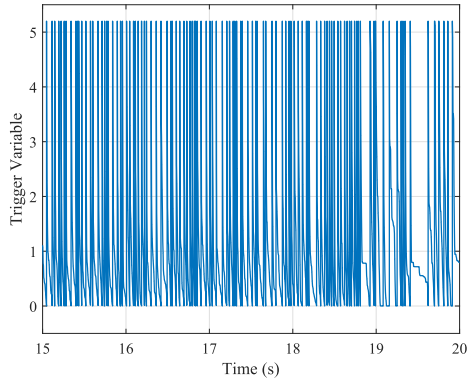

Fig. 8. Trigger variable $\eta_1(t)$ for converter 1, which decreases from β_1 (namely, 5.2) to 0 between two successive event times and is reset from 0 to β_1 at each event time.

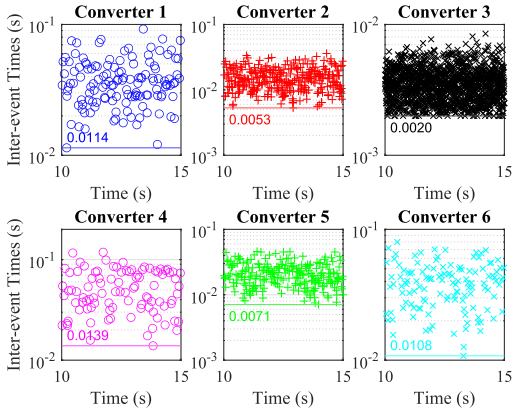

Fig. 9. Interevent times $t^i_{k+1} - t^i_k$, for converters i, $i = 1, 2, \ldots, 6$, and observed MIETs indicated with horizontal lines.

Fig. 9, are 0.0114, 0.0053, 0.0020, 0.0139, 0.0071, and 0.0108 s, respectively. Additionally, MIETs for converters i, $i = 1, 2, \ldots, 6$, as given by (17), are 0.0018, 0.0009, 0.0004, 0.0018, 0.0011, and 0.0015 s, respectively. It is clear that the observed MIETs are larger than the corresponding calculated MIETs. This implies that the MIET found by (17) is conservative.

3) Communication Delay: Consider the case when the communication links among converters are subject to a common communication delay. In this case, the impact of the communication delay on the control performance is studied. The proposed distributed dynamic ETC strategy in the presence of the communication delay is conducted under the same setting as in Figs. 5 and 6. The converter output currents (in p.u.) and the global average voltage under different communication delays are shown in Fig. 10. As seen, the proportional current sharing can be well achieved when the communication delay is small. As the communication delay increases, the converter output currents (in p.u.) begin to oscillate. In addition, the global average voltage deviates further from the nominal value, 48 V, as the communication delay increases. The communication delays given in Fig. 10 are the time delays in information transmissions that the proposed control strategy could tolerate under the considered parameter setting. By conducting experiments with different communication delays, one can find an approximate delay margin for the stable operation. The delay margin is

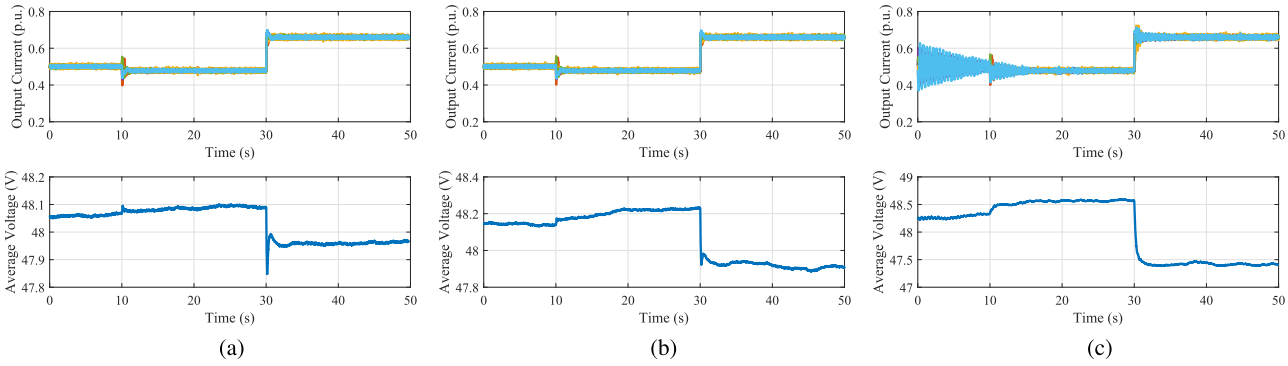

Fig. 10. Experimental results under different communication delays, which are the time-delays in information transmissions through all the communication links among converters. (a) Communication delay: 0.005 s. (b) Communication delay: 0.010 s. (c) Communication delay: 0.037 s.

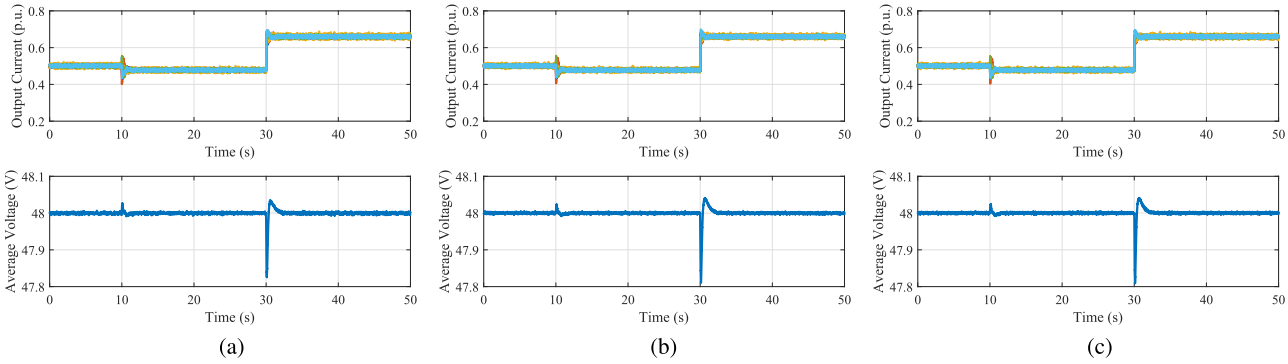

Fig. 11. Experimental results under different control strategies. (a) Dynamic ETC. (b) Static ETC. (c) Periodic sampling.

TABLE IV
NUMBER OF INFORMATION TRANSMISSIONS FOR EACH CONVERTER UNDER DIFFERENT CONTROL STRATEGIES

Control strategy	Number of information transmissions for converter i					
	$i=1$	$i=2$	$i=3$	$i=4$	$i=5$	$i=6$
Dynamic ETC	3384	8639	38017	2804	5914	3784
Static ETC	19 519	30 802	65 395	17 523	27 319	22 605
Periodic sampling	50 000	50 000	50 000	50 000	50 000	50 000

the maximum allowable time delay before the control system becomes unstable. Experimental results show that the delay margin of the proposed control strategy is about 0.037 s.

4) Comparison With Existing Methods: The proposed dynamic ETC strategy is compared with the static ETC strategy in [13] and the conventional periodic sampling control strategy. Due to the tradeoff in case 2), the number of information transmissions is compared for different control strategies in the case when their dynamic responses are similar. Consider the same load conditions in Table II, and choose the same controller parameters as in case 1). For the static ETC strategy in [13], choose the trigger parameters $\varepsilon_1 = \varepsilon_2 = 0.05$ and $\sigma = 0.99$. For the conventional periodic sampling control strategy, each converter sends samples of its output current (in p.u.) $I_i(t)/I_{ci}$ to its neighbors at the sampling period of 1 ms. Fig. 11 shows the bus voltage, observed by each converter, and the global average voltage under different control strategies. Table IV shows the number of information transmissions over the communication network for each converter during the time-interval [0,50] s. It

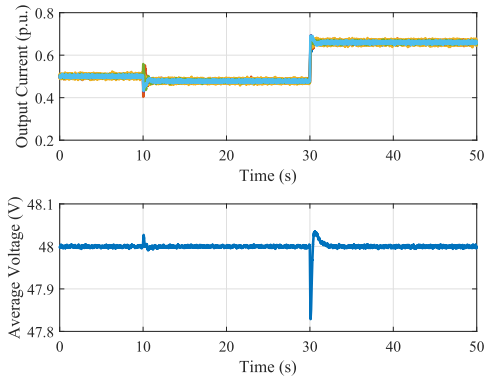

Fig. 12. Experimental results with different switching frequencies among converters.

can be seen from Fig. 11 that the control performance under these control strategies is similar. Nevertheless, the communication burden in the case of dynamic ETC is significantly reduced. The proposed ETC strategy outperforms the other two control strategies in terms of reducing the communication burden, while maintaining a similar control performance.

5) Effect of the Switching Frequency: In the preceding settings, all converters had the same switching frequency of 20 kHz. We now consider the case where converters have different switching frequencies. The proposed dynamic ETC strategy is implemented on converters $1, 2, \ldots, 6$, with respective switching frequencies of 20, 20, 50, 50, 100, and 100 kHz. The experimental results, under these switching frequencies, are shown in

Fig. 12. The dynamic response in Fig. 12 is indistinguishable as that in Fig. 11(a). Given that the smallest MIET is still much larger than the switching interval, i.e., the communication among converters happens much slower than converters' switching, the impact of converter's switching frequency on the controller performance can be negligible.

VI. Conclusion

We have studied distributed event-triggered secondary control of dc microgrids by proposing a new distributed dynamic ETM. The resulting distributed ETC law and distributed dynamic ETM simultaneously achieve the proportional current sharing and global voltage regulation. One key merit of the proposed dynamic ETM over existing static ones is the guarantee of the existence of a positive tunable MIET. The proposed control method has been validated on a dc microgrid testbed in a C-HIL environment. Experimental results show that the proposed dynamic ETM can significantly reduce the communication burden compared to the existing static ETM and the conventional periodic sampling. Moreover, the control strategy in this article does not require any global information of the communication graph or the closed-loop system dynamics.

Appendix
Proof of Lemma 1

Under Assumption 1, the Laplacian matrices $L_{\rm e}$ and $L_{\rm c}$ are real, symmetric, and hence, diagonalizable. According to [27, Th. 1.3.12], the Laplacian matrices $L_{\rm e}$ and $L_{\rm c}$ are commutative if and only if they are simultaneously diagonalizable. Thus, under Assumption 2, there exists a nonsingular matrix S such that $D_{\rm e} \triangleq S^{-1}L_{\rm e}S$ and $D_{\rm c} \triangleq S^{-1}L_{\rm c}S$ are both diagonal. Under Assumption 1, the Laplacian matrices $L_{\rm e}$ and $L_{\rm c}$ have a simple zero eigenvalue, with other eigenvalues being strictly positive [24]. By properly arranging the columns of S, the diagonal matrices $D_{\rm e}$ and $D_{\rm c}$ are expressed as

$$D_{\rm e} = {\rm diag}\{0, \lambda_{\rm e2}, \lambda_{\rm e3}, \ldots, \lambda_{{\rm e}N}\} \tag{35}$$

$$D_{\rm c} = {\rm diag}\{0, \lambda_{\rm c2}, \lambda_{\rm c3}, \ldots, \lambda_{{\rm c}N}\} \tag{36}$$

where $0, \lambda_{\rm e2}, \lambda_{\rm e3}, \ldots, \lambda_{{\rm e}N}$ are the eigenvalues of $L_{\rm e}$, and $0, \lambda_{\rm c2}, \lambda_{\rm c3}, \ldots, \lambda_{{\rm c}N}$ are the eigenvalues of $L_{\rm c}$. Let $D_{\rm Q} = {\rm diag}\{\lambda_1, \lambda_{\rm e2}/\lambda_{\rm c2}, \lambda_{\rm e3}/\lambda_{\rm c3}, \ldots, \lambda_{{\rm e}N}/\lambda_{{\rm c}N}\} > 0$, with $\lambda_1 > 0$. Then, $D_{\rm e} = D_{\rm c}D_{\rm Q}$. Furthermore, $L_{\rm e}$ can be rewritten as

$$L_{\rm e} = SD_{\rm e}S^{-1} = SD_{\rm c}S^{-1}SD_{\rm Q}S^{-1} = L_{\rm c}Q \tag{37}$$

where $Q \triangleq SD_{\rm Q}S^{-1}$. Then, Q is a positive-definite matrix.

Appendix B
Proof of Theorem 1

Consider the evolution of the trigger variable $\eta_i(t)$ over the time-interval $[t_k^i, t_{k+1}^i)$ in the following two cases. On the one hand, when $e_i(t) \neq 0$, $\varpi_i(t)$ is lower bounded by

$$\begin{aligned}
\varpi_i(t) =& \ \frac{\sigma_i}{I_{{\rm c}i}} K_I \left(\lambda_{\min}(Q) - 3\kappa d_i\right) \frac{\hat{\delta}_{Ii}^2(t)}{e_i^2(t)} \\
&+ \frac{2\sigma_i}{I_{ci}} K_V \left(\frac{K_V \lambda_{\min}(Q)}{K - K_I} - 2\kappa d_i\right) \frac{\bar{\delta}_{Vi}^2(t)}{e_i^2(t)} \\
&- \frac{2}{\kappa I_{ci}} \left(K_I + K_V\right) d_i \left(1 + \eta_i^2(t)\right) \\
\geq& \ - \frac{2}{\kappa I_{ci}} \left(K_I + K_V\right) d_i \left(1 + \eta_i^2(t)\right) \\
\geq& \ - \frac{2}{\kappa I_{ci}} \left(K_I + K_V\right) d_i \left(\eta_i(t) + 1\right)^2 \\
=& \ - \frac{1}{\kappa} \gamma_i \left(\eta_i(t) + 1\right)^2
\end{aligned} \tag{38}$$

where $\eta_i(t) \geq 0$ and $\gamma_i = (2/I_{ci})(K_I + K_V)d_i$ have been used. Then, one has

$$\begin{aligned}
\dot{\eta}_i(t) &= \min\{\varpi_i(t), 0\} - \alpha_i \\
&\geq -\frac{1}{\kappa} \gamma_i \left(\eta_i(t) + 1\right)^2 - \alpha_i.
\end{aligned} \tag{39}$$

On the other hand, when $e_i(t) = 0$, $\dot{\eta}_i(t)$ satisfies

$$\dot{\eta}_i(t) = -\alpha_i \geq -\frac{1}{\kappa} \gamma_i \left(\eta_i(t) + 1\right)^2 - \alpha_i. \tag{40}$$

Combining (39) and (40) yields

$$\dot{\eta}_i(t) \geq -\frac{1}{\kappa} \gamma_i \left(\eta_i(t) + 1\right)^2 - \alpha_i \tag{41}$$

for $t \in [t_k^i, t_{k+1}^i)$. Thus, according to the comparison lemma [28, Lemma 3.4], $\eta_i(t) \geq \phi_i(t)$, for $t \in [t_k^i, t_{k+1}^i)$, where $\phi_i(t)$ satisfies the following differential equation:

$$\dot{\phi}_i(t) = -\frac{1}{\kappa} \gamma_i \left(\phi_i(t) + 1\right)^2 - \alpha_i \tag{42}$$

with $\phi_i(t_k^i) = \beta_i$. Let $\chi_i(t) = \sqrt{\gamma_i/(\kappa\alpha_i)}(\phi_i(t) + 1)$. Then, it follows from (42) that

$$-\sqrt{\frac{\kappa}{\alpha_i\gamma_i}} \frac{\dot{\chi}_i(t)}{\chi_i^2(t) + 1} = 1. \tag{43}$$

Integrating both sides of (43) from t_k^i to t yields

$$\begin{aligned}
&t - t_k^i \\
&= \sqrt{\frac{\kappa}{\alpha_i\gamma_i}} \left(\arctan\left(\chi_i(t_k^i)\right) - \arctan\left(\chi_i(t)\right)\right) \\
&= \sqrt{\frac{\kappa}{\alpha_i\gamma_i}} \left[\arctan\left(\sqrt{\frac{\gamma_i}{\kappa\alpha_i}} \left(\beta_i + 1\right)\right)\right. \\
&\quad \left. - \arctan\left(\sqrt{\frac{\gamma_i}{\kappa\alpha_i}} \left(\phi_i(t) + 1\right)\right)\right].
\end{aligned} \tag{44}$$

Since $\eta_i(t) \geq \phi_i(t)$ for $t \in [t_k^i, t_{k+1}^i)$, the interevent time $t_{k+1}^i - t_k^i$ is lower bounded by the amount of time that it takes for $\phi_i(t)$ to drop from β_i to 0. Thus, by (44), it is concluded that the lower bound of $t_{k+1}^i - t_k^i$ is given by τ_i in (17).

Appendix C
Proof of Theorem 2

Consider the Lyapunov function candidate

$$W(t) = W_1(t) + W_2(t) + W_3(t) \tag{45}$$

where

$$W_1(t) = \frac{1}{2} I^{\mathrm{T}}(t) I_{\mathrm{c}}^{-1} I(t) + \frac{1}{2} e^{\mathrm{T}}(t) \eta(t) I_{\mathrm{c}} e(t) \tag{46a}$$

$$W_2(t) = \frac{1}{2} \delta_V^2(t) \tag{46b}$$

$$W_3(t) = \frac{1}{2} \frac{K_V}{K - K_I} \bar{\delta}_V^{\mathrm{T}}(t) Q \bar{\delta}_V(t) \tag{46c}$$

with $\eta \triangleq \mathrm{diag}\{\eta_1, \eta_2, \ldots, \eta_N\}$ and $Q > 0$ given in Lemma 1. The time-derivatives of $W_i, i = 1, 2, 3$ along the trajectory of the closed-loop system (24a)–(24h) on each time-interval (t_l, t_{l+1}), $l \in \mathbb{N}$ are

$$\begin{aligned}
\dot{W}_1(t) = \; & I^{\mathrm{T}}(t) I_{\mathrm{c}}^{-1} \dot{I}(t) + e^{\mathrm{T}}(t) \eta(t) I_{\mathrm{c}} \dot{e}(t) \\
& + \frac{1}{2} e^{\mathrm{T}}(t) \dot{\eta}(t) I_{\mathrm{c}} e(t) \\
= \; & - \frac{1}{2} K_I \delta_I^{\mathrm{T}}(t) Q \delta_I(t) - \frac{1}{2} K_I \delta_I^{\mathrm{T}}(t) L_{\mathrm{e}} e(t) \\
& - \frac{1}{2} K_I \hat{\delta}_I^{\mathrm{T}}(t) Q \hat{\delta}_I(t) + \frac{1}{2} K_I e^{\mathrm{T}}(t) L_{\mathrm{e}} \hat{\delta}_I(t) \\
& - K_V \hat{\delta}_I^{\mathrm{T}}(t) Q \bar{\delta}_V(t) + K_V e^{\mathrm{T}}(t) L_{\mathrm{e}} \bar{\delta}_V(t) \\
& + K_I e^{\mathrm{T}}(t) \eta(t) L_{\mathrm{e}} \hat{\delta}_I(t) + K_V e^{\mathrm{T}}(t) \eta(t) L_{\mathrm{e}} \bar{\delta}_V(t) \\
& + \frac{1}{2} e^{\mathrm{T}}(t) \dot{\eta}(t) I_{\mathrm{c}} e(t)
\end{aligned} \tag{47}$$

$$\dot{W}_2(t) = \delta_V(t) \dot{\delta}_V(t) = -K_V \delta_V^2(t) \tag{48}$$

$$\begin{aligned}
\dot{W}_3(t) = \; & \frac{K_V}{K - K_I} \bar{\delta}_V^{\mathrm{T}}(t) Q \dot{\bar{\delta}}_V(t) \\
= \; & \frac{K_V}{K - K_I} \bar{\delta}_V^{\mathrm{T}}(t) Q \left[(K - K_I) \hat{\delta}_I(t) - K_V \bar{\delta}_V(t) \right] \\
= \; & - \frac{K_V^2}{K - K_I} \bar{\delta}_V^{\mathrm{T}}(t) Q \bar{\delta}_V(t) + K_V \hat{\delta}_I^{\mathrm{T}}(t) Q \bar{\delta}_V(t)
\end{aligned} \tag{49}$$

where (7), (21a), and (21b) have been used to derive (47). Substituting (47)–(49) into $\dot{W}(t)$ yields

$$\begin{aligned}
\dot{W}(t) = \; & - \frac{1}{2} K_I \delta_I^{\mathrm{T}}(t) Q \delta_I(t) - \frac{1}{2} K_I \delta_I^{\mathrm{T}}(t) L_{\mathrm{e}} e(t) \\
& - \frac{1}{2} K_I \hat{\delta}_I^{\mathrm{T}}(t) Q \hat{\delta}_I(t) + \frac{1}{2} K_I e^{\mathrm{T}}(t) L_{\mathrm{e}} \hat{\delta}_I(t) \\
& + K_V e^{\mathrm{T}}(t) L_{\mathrm{e}} \bar{\delta}_V(t) + K_I e^{\mathrm{T}}(t) \eta(t) L_{\mathrm{e}} \hat{\delta}_I(t) \\
& + K_V e^{\mathrm{T}}(t) \eta(t) L_{\mathrm{e}} \bar{\delta}_V(t) + \frac{1}{2} e^{\mathrm{T}}(t) \dot{\eta}(t) I_{\mathrm{c}} e(t) \\
& - K_V \delta_V^2(t) - \frac{K_V^2}{K - K_I} \bar{\delta}_V^{\mathrm{T}}(t) Q \bar{\delta}_V(t)
\end{aligned} \tag{50}$$

for $t \in (t_l, t_{l+1})$. By using the Young's inequality $ab \leq a^2/(2\kappa) + (\kappa b^2)/2$, with $\kappa > 0$, one has

$$\begin{aligned}
& x^{\mathrm{T}}(t) L_{\mathrm{e}} y(t) \\
= \; & \sum_{i=1}^{N} x_i(t) \sum_{j=1}^{N} w_{ij} \left(y_i(t) - y_j(t) \right) \\
= \; & \sum_{i=1}^{N} d_i x_i(t) y_i(t) - \sum_{i=1}^{N} \sum_{j=1}^{N} w_{ij} x_i(t) y_j(t) \\
\leq \; & \frac{1}{\kappa} \sum_{i=1}^{N} d_i x_i^2(t) + \frac{\kappa}{2} \sum_{i=1}^{N} d_i y_i^2(t) \\
& + \frac{\kappa}{2} \sum_{i=1}^{N} \sum_{j=1}^{N} w_{ij} y_j^2(t)
\end{aligned} \tag{51}$$

where $d_i = \sum_{j=1}^{N} w_{ij}$. Since $w_{ij} = w_{ji}, i, j \in \mathcal{V}$, then

$$\sum_{i=1}^{N} \sum_{j=1}^{N} w_{ij} y_j^2(t) = \sum_{i=1}^{N} \sum_{j=1}^{N} w_{ij} y_i^2(t) = \sum_{i=1}^{N} d_i y_i^2(t). \tag{52}$$

Substituting (52) into (51) yields

$$x^{\mathrm{T}}(t) L_{\mathrm{e}} y(t) \leq \frac{1}{\kappa} \sum_{i=1}^{N} d_i x_i^2(t) + \kappa \sum_{i=1}^{N} d_i y_i^2(t). \tag{53}$$

Using (53), one obtains the following inequalities:

$$\begin{aligned}
& - \frac{1}{2} K_I \delta_I^{\mathrm{T}}(t) L_{\mathrm{e}} e(t) \\
\leq \; & \frac{1}{2\kappa} K_I \sum_{i=1}^{N} d_i e_i^2(t) + \frac{1}{2} \kappa K_I \sum_{i=1}^{N} d_i \delta_{Ii}^2(t)
\end{aligned} \tag{54}$$

$$\begin{aligned}
& \frac{1}{2} K_I e^{\mathrm{T}}(t) L_{\mathrm{e}} \hat{\delta}_I(t) + K_V e^{\mathrm{T}}(t) L_{\mathrm{e}} \bar{\delta}_V(t) \\
\leq \; & \frac{1}{2\kappa} K_I \sum_{i=1}^{N} d_i e_i^2(t) + \frac{1}{2} \kappa K_I \sum_{i=1}^{N} d_i \hat{\delta}_{Ii}^2(t) \\
& + \frac{1}{\kappa} K_V \sum_{i=1}^{N} d_i e_i^2(t) + \kappa K_V \sum_{i=1}^{N} d_i \bar{\delta}_{Vi}^2(t)
\end{aligned} \tag{55}$$

$$\begin{aligned}
& K_I e^{\mathrm{T}}(t) \eta(t) L_{\mathrm{e}} \hat{\delta}_I(t) + K_V e^{\mathrm{T}}(t) \eta(t) L_{\mathrm{e}} \bar{\delta}_V(t) \\
\leq \; & \frac{1}{\kappa} K_I \sum_{i=1}^{N} d_i \eta_i^2(t) e_i^2(t) + \kappa K_I \sum_{i=1}^{N} d_i \hat{\delta}_{Ii}^2(t) \\
& + \frac{1}{\kappa} K_V \sum_{i=1}^{N} d_i \eta_i^2(t) e_i^2(t) + \kappa K_V \sum_{i=1}^{N} d_i \bar{\delta}_{Vi}^2(t).
\end{aligned} \tag{56}$$

Substitution of (54)–(56) into (50) yields

$$\begin{aligned}
\dot{W}(t) \leq \; & - \frac{1}{2} K_I \sum_{i=1}^{N} \left(\lambda_{\min}(Q) - \kappa d_i \right) \delta_{Ii}^2(t) - K_V \delta_V^2(t) \\
& - \frac{1}{2} K_I \sum_{i=1}^{N} \left(\lambda_{\min}(Q) - 3\kappa d_i \right) \hat{\delta}_{Ii}^2(t) \\
& - K_V \sum_{i=1}^{N} \left(\frac{K_V \lambda_{\min}(Q)}{K - K_I} - 2\kappa d_i \right) \bar{\delta}_{Vi}^2(t) \\
& + \frac{1}{\kappa} \left(K_I + K_V \right) \sum_{i=1}^{N} d_i \left(1 + \eta_i^2(t) \right) e_i^2(t)
\end{aligned}$$

$$+\frac{1}{2}\sum_{i=1}^{N} I_{ci}\dot{\eta}_i(t)e_i^2(t)$$

$$\triangleq \sum_{i=1}^{N} W_i(t) \tag{57}$$

for $t \in (t_l, t_{l+1})$. Let κ be chosen such that

$$0 < \kappa < \min\left\{\frac{\lambda_{\min}(Q)}{3\max_{i\in\mathcal{V}} d_i}, \frac{K_V\lambda_{\min}(Q)}{2(K-K_I)\max_{i\in\mathcal{V}} d_i}\right\}. \tag{58}$$

Then, $\lambda_{\min}(Q) - \kappa d_i > 0$, $\lambda_{\min}(Q) - 3\kappa d_i > 0$, and $K_V\lambda_{\min}(Q)/(K-K_I) - 2\kappa d_i > 0$.

Consider the two cases when $e_i(t) \neq 0$ and $e_i(t) = 0$. When $e_i(t) \neq 0$, the dynamics of $\eta_i(t)$ satisfy

$$\begin{aligned}\dot{\eta}_i(t) <\ \varpi_i(t) = {}& \frac{\sigma_i}{I_{ci}} K_I\left(\lambda_{\min}(Q) - 3\kappa d_i\right)\frac{\hat{\delta}_{Ii}^2(t)}{e_i^2(t)} \\ &+ \frac{2\sigma_i}{I_{ci}} K_V\left(\frac{K_V\lambda_{\min}(Q)}{K-K_I} - 2\kappa d_i\right)\frac{\bar{\delta}_{Vi}^2(t)}{e_i^2(t)} \\ &- \frac{2}{\kappa I_{ci}}\left(K_I + K_V\right) d_i\left(1+\eta_i^2(t)\right)\end{aligned} \tag{59}$$

with $0 < \sigma_i < 1$. It follows from (59) that $W_i(t)$ in (57) satisfies

$$\begin{aligned}W_i(t) <\ & -\frac{1}{2}K_I\left(\lambda_{\min}(Q) - \kappa d_i\right)\delta_{Ii}^2(t) - K_V\delta_{Vi}^2(t) \\ & -\frac{1}{2}K_I\left(1-\sigma_i\right)\left(\lambda_{\min}(Q) - 3\kappa d_i\right)\hat{\delta}_{Ii}^2(t) \\ & - K_V\left(1-\sigma_i\right)\left(\frac{K_V\lambda_{\min}(Q)}{K-K_I} - 2\kappa d_i\right)\bar{\delta}_{Vi}^2(t).\end{aligned} \tag{60}$$

For the case when $e_i(t) = 0$, $W_i(t)$ in (57) becomes

$$\begin{aligned}W_i(t) = & -\frac{1}{2}K_I\left(\lambda_{\min}(Q) - \kappa d_i\right)\delta_{Ii}^2(t) - K_V\delta_{Vi}^2(t) \\ & -\frac{1}{2}K_I\left(\lambda_{\min}(Q) - 3\kappa d_i\right)\hat{\delta}_{Ii}^2(t) \\ & - K_V\left(\frac{K_V\lambda_{\min}(Q)}{K-K_I} - 2\kappa d_i\right)\bar{\delta}_{Vi}^2(t).\end{aligned} \tag{61}$$

Combining (60) and (61), one obtains from (57) that

$$\begin{aligned}\dot{W}(t) &\le \sum_{i=1}^{N} W_i(t) \\ &\le -\frac{1}{2}K_I\min_{i\in\mathcal{V}}\left\{\left(\lambda_{\min}(Q) - \kappa d_i\right)\right\}\delta_I^2(t) - K_V\delta_V^2(t) \\ &\quad -\frac{1}{2}K_I\min_{i\in\mathcal{V}}\left\{\left(1-\sigma_i\right)\left(\lambda_{\min}(Q) - 3\kappa d_i\right)\right\}\hat{\delta}_I^2(t) \\ &\quad - K_V\min_{i\in\mathcal{V}}\left\{\left(1-\sigma_i\right)\left(\frac{K_V\lambda_{\min}(Q)}{K-K_I} - 2\kappa d_i\right)\right\}\bar{\delta}_V^2(t) \\ &\le 0\end{aligned} \tag{62}$$

for $t \in (t_l, t_{l+1})$. Furthermore, it can be verified that $W(t_l^+) - W(t_l^-) = 0$. By Theorem 1, the Zeno behavior is ruled out for each converter, which means that $\lim_{k\to\infty} t_k^i = \infty$, for all $i \in \mathcal{V}$. Hence, $\lim_{l\to\infty} t_l = \infty$. By the invariant set theorem [29, Th. 2.3], one can conclude that $\delta_I(t) \to 0$, $\delta_V(t) \to 0$, $\hat{\delta}_I(t) \to 0$, and $\bar{\delta}_V(t) \to 0$, as $t \to \infty$.

REFERENCES

[1] T. Dragičević, X. Lu, J. C. Vasquez, and J. M. Guerrero, "DC microgrids-Part I: A review of control strategies and stabilization techniques," *IEEE Trans. Power Electron.*, vol. 31, no. 7, pp. 4876–4891, Jul. 2016.

[2] T. Dragičević, X. Lu, J. C. Vasquez, and J. M. Guerrero, "DC microgrids-Part II: A review of power architectures, applications, and standardization issues," *IEEE Trans. Power Electron.*, vol. 31, no. 5, pp. 3528–3549, May 2016.

[3] S. Moayedi and A. Davoudi, "Unifying distributed dynamic optimization and control of islanded DC microgrids," *IEEE Trans. Power Electron.*, vol. 32, no. 3, pp. 2329–2346, Mar. 2017.

[4] S. Anand, B. G. Fernandes, and J. Guerrero, "Distributed control to ensure proportional load sharing and improve voltage regulation in low-voltage DC microgrids," *IEEE Trans. Power Electron.*, vol. 28, no. 4, pp. 1900–1913, Apr. 2013.

[5] V. Nasirian, S. Moayedi, A. Davoudi, and F. L. Lewis, "Distributed cooperative control of DC microgrids," *IEEE Trans. Power Electron.*, vol. 30, no. 4, pp. 2288–2303, Apr. 2015.

[6] P. Tabuada, "Event-triggered real-time scheduling of stabilizing control tasks," *IEEE Trans. Autom. Control*, vol. 52, no. 9, pp. 1680–1685, Sep. 2007.

[7] W. P. M. H. Heemels, K. H. Johansson, and P. Tabuada, "An introduction to event-triggered and self-triggered control," in *Proc. 51st IEEE Conf. Decis. Control*, 2012, pp. 3270–3285.

[8] S. Sahoo and S. Mishra, "An adaptive event-triggered communication-based distributed secondary control for DC microgrids," *IEEE Trans. Smart Grid*, vol. 9, no. 6, pp. 6674–6683, Nov. 2018.

[9] D. Pullaguram, S. Mishra, and N. Senroy, "Event-triggered communication based distributed control scheme for DC microgrid," *IEEE Trans. Power Syst.*, vol. 33, no. 5, pp. 5583–5593, Sep. 2018.

[10] R. Han, L. Meng, J. M. Guerrero, and J. C. Vasquez, "Distributed nonlinear control with event-triggered communication to achieve current-sharing and voltage regulation in DC microgrids," *IEEE Trans. Power Electron.*, vol. 33, no. 7, pp. 6416–6433, Jul. 2018.

[11] B. Fan, J. Peng, Q. Yang, and W. Liu, "Distributed periodic event-triggered algorithm for current sharing and voltage regulation in DC microgrids," *IEEE Trans. Smart Grid*, vol. 11, no. 1, pp. 577–589, Jan. 2020.

[12] F. Guo, L. Wang, C. Wen, D. Zhang, and Q. Xu, "Distributed voltage restoration and current sharing control in islanded DC microgrid systems without continuous communication," *IEEE Trans. Ind. Electron.*, vol. 67, no. 4, pp. 3043–3053, Jul. 2019.

[13] J. Peng, B. Fan, Q. Yang, and W. Liu, "Distributed event-triggered control of DC microgrids," *IEEE Syst. J.*, vol. 15, no. 2, pp. 2504–2514, Jun. 2021.

[14] Y. Fan, G. Hu, and M. Egerstedt, "Distributed reactive power sharing control for microgrids with event-triggered communication," *IEEE Trans. Control Syst. Technol.*, vol. 25, no. 1, pp. 118–128, Jan. 2017.

[15] L. Ding, Q.-L. Han, and X.-M. Zhang, "Distributed secondary control for active power sharing and frequency regulation in islanded microgrids using an event-triggered communication mechanism," *IEEE Trans. Ind. Inform.*, vol. 15, no. 7, pp. 3910–3922, Jul. 2019.

[16] Y. Xie and Z. Lin, "Distributed event-triggered secondary voltage control for microgrids with time delay," *IEEE Trans. Syst., Man, Cybern. Syst.*, vol. 49, no. 8, pp. 1582–1591, Aug. 2019.

[17] A. Girard, "Dynamic triggering mechanisms for event-triggered control," *IEEE Trans. Autom. Control*, vol. 60, no. 7, pp. 1992–1997, Jul. 2015.

[18] V. Dolk, D. P. Borgers, and W. P. M. H. Heemels, "Dynamic event-triggered control: Tradeoffs between transmission intervals and performance," in *Proc. 53rd IEEE Conf. Decis. Control*, 2014, pp. 2764–2769.

[19] J. Berneburg and C. Nowzari, "Distributed dynamic event-triggered coordination with a designable minimum inter-event time," in *Proc. 2019 Amer. Control Conf.*, 2019, pp. 1424–1429.

[20] Y.-Y. Qian, L. Liu, and G. Feng, "Output consensus of heterogeneous linear multi-agent systems with adaptive event-triggered control," *IEEE Trans. Autom. Control*, vol. 64, no. 6, pp. 2606–2613, Jun. 2019.

[21] Y.-Y. Qian and Y. Wan, "Design of distributed adaptive event-triggered consensus control strategies with positive minimum inter-event times," *Automatica*, vol. 133, Nov. 2021, Art. no. 109837.

[22] S. Anand and B. G. Fernandes, "Reduced-order model and stability analysis of low-voltage DC microgrid," *IEEE Trans. Ind. Electron.*, vol. 60, no. 11, pp. 5040–5049, Nov. 2013.
[23] V. Nasirian, A. Davoudi, F. L. Lewis, and J. M. Guerrero, "Distributed adaptive droop control for DC distribution systems," *IEEE Trans. Energy Convers.*, vol. 29, no. 4, pp. 944–956, Dec. 2014.
[24] R. Olfati-Saber, J. A. Fax, and R. M. Murray, "Consensus and cooperation in networked multi-agent systems," *Proc. IEEE*, vol. 95, no. 1, pp. 215–233, Jan. 2007.
[25] Q. Shafiee, T. Dragičević, J. C. Vasquez, and J. M. Guerrero, "Hierarchical control for multiple DC-microgrids clusters," *IEEE Trans. Energy Convers.*, vol. 29, no. 4, pp. 922–933, Dec. 2014.
[26] V. Nasirian, A. P. Yadav, F. L. Lewis, and A. Davoudi, "Distributed assistive control of power buffers in DC microgrids," *IEEE Trans. Energy Convers.*, vol. 32, no. 4, pp. 1396–1406, Dec. 2017.
[27] R. A. Horn and C. R. Johnson, *Matrix Analysis*, 2nd ed. Cambridge, U.K.: Cambridge Univ. Press, 2013.
[28] H. K. Khalil, *Nonlinear Systems*, 3rd ed. Upper Saddle River, NJ, USA: Prentice-Hall, 2002.
[29] W. M. Haddad, V. Chellaboina, and S. G. Nersesov, *Impulsive and Hybrid Dynamical Systems: Stability, Dissipativity, and Control*. Princeton, NJ, USA: Princeton Univ. Press, 2006.

Yang-Yang Qian (Member, IEEE) received the B.Eng. degree in automation from the Xi'an University of Posts and Telecommunications, Xi'an, China, in 2012, the M.Eng. degree in control science and engineering from the Harbin Institute of Technology, Harbin, China, in 2015, and the Ph.D. degree from the Department of Biomedical Engineering, City University of Hong Kong, Hong Kong, in 2019.

He is currently a Postdoctoral Research Associate with the Department of Electrical Engineering, University of Texas at Arlington, Arlington, TX, USA. His research interests include distributed control, event-triggered control, adaptive control, multi-agent systems, and microgrids.

Abhiram V. P. Premakumar (Graduate Student Member, IEEE) received the B.Tech. degree in electrical and electronics engineering from the College of Engineering, Trivandrum, Kerala, India, in 2016, and the M.Tech. degree in electrical engineering from the Indian Institute of Technology, Kanpur, Kanpur, Uttar Pradesh, India, in 2019. He is currently working toward the Ph.D. degree in electrical engineering with the University of Texas at Arlington, Arlington, TX, USA.

His research interests include modeling, control, and optimization of power electronics systems.

Yan Wan (Senior Member, IEEE) received the Ph.D. degree in electrical engineering from Washington State University, Vancouver, WA, USA, in 2009, and then did postdoctoral training with the University of California, Santa Barbara, Santa Barbara, CA, USA.

She is currently a Distinguished University Professor with the Electrical Engineering Department, University of Texas at Arlington, Arlington, TX, USA. Her research interests include the modeling, evaluation, and control of large-scale dynamical networks, cyber-physical systems, stochastic networks, decentralized control, and their applications to smart grids, urban aerial mobility, autonomous driving, and robot networking.

Dr. Wan is currently a member of the Board of Governors of the IEEE Control Systems Society (CSS). She also serves in the Technical Committees of AIAA Intelligent Systems, IEEE CSS Nonlinear Systems and Control, and IEEE CSS Networks and Communication Systems.

Zongli Lin (Fellow, IEEE) received the B.S. degree in mathematics and computer science from Xiamen University, Xiamen, China, in 1983, the master of engineering degree in automatic control from Chinese Academy of Space Technology, Beijing, China, in 1989, and the Ph.D. degree in electrical and computer engineering from Washington State University, Pullman, WA, USA, in 1994.

He is the Ferman W. Perry Professor with the School of Engineering and Applied Science and a Professor of Electrical and Computer Engineering with University of Virginia, Charlottesville, VA, USA. His research interests include nonlinear control, robust control, and control applications.

Dr. Lin is a Fellow of International Federation of Automatic Control, and the American Association for the Advancement of Science. He was an Associate Editor for IEEE TRANSACTIONS ON AUTOMATIC CONTROL, from 2001 to 2003, IEEE/ASME TRANSACTIONS ON MECHATRONICS, from 2006 to 2009, and *IEEE Control Systems Magazine*, from 2005 to 2012. He currently serves on the editorial boards of several journals and book series, including *Automatica*, *Systems & Control Letters*, and Springer/Birkhauser book series Control Engineering. He was elected a member of the Board of Governors of the IEEE Control Systems Society, from 2008 to 2010, and from 2019 to 2021, and chaired the IEEE Control Systems Society Technical Committee on Nonlinear Systems and Control, from 2013 to 2015. He has served on the operating committees of several conferences and was a general chair of the 2012 and 2018 International Symposia on Magnetic Bearings and the program chair of the 2018 American Control Conference.

Yacov A. Shamash (Life Fellow, IEEE) received the Ph.D. degree in electrical engineering from the Imperial College of Sciences and Technology, London, U.K., in 1973.

He is a Professor of Electrical and Computer Engineering with Stony Brook University, Stony Brook, NY, USA, where he was the founder of the New York State Center for Excellence in Wireless and in Information Technology, and the New York State Center for Excellence in Advanced Energy Research and Technology. He has previously served as the Vice President for Economic Development, the Dean of Engineering and Applied Sciences, and the Dean of the Harriman School for Management and Policy, Stony Brook University. Prior to joining Stony Brook University, he developed and directed the National Science Foundation Industry/University Cooperative Research Center for the Design of Analog/Digital Integrated Circuits and also served as Chairman of the Electrical and Computer Engineering Department, Washington State University, Pullman, WA, USA. He serves on the Board of Directors of Comtech Telecommunications Corp., Huntington, NY, USA, KeyTronic Corp., Spokane, WA, USA, and Applied DNA Sciences, Inc., Stony Brook, NY, USA.

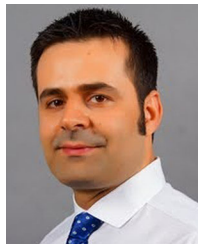

Ali Davoudi (Senior Member, IEEE) received the Ph.D. degree in electrical and computer engineering from the University of Illinois, Urbana-Champaign, IL, USA, in 2010.

He is currently a Professor with the Electrical Engineering Department, University of Texas at Arlington, Arlington, TX, USA. His research interests include modeling, control, and optimization of power electronics systems.

Dr. Davoudi is an Associate Editor for the IEEE TRANSACTIONS ON POWER ELECTRONICS, and an Editor for the IEEE TRASACTIONS ON ENERGY CONVERSION, as well as IEEE POWER ENGINEERING LETTERS.